A Distributed Beam Loss Monitor for the Australian Synchrotron

Paul J. Giansiracusa[a,*], Mark J. Boland[b,c], Eva Barbara Holzer[d], Maria Kastriotou[d,e], Greg S. LeBlanc[f], Thomas G. Lucas[a], Eduardo Nebot del Busto[d,e], Roger P. Rassool[a], Matteo Volpi[a], Carsten P. Welsch[e]

[a]*School of Physics, The University of Melbourne, Parkville, Australia*
[b]*Department of Physics and Engineering Physics, University of Saskatchewan, 116 Science Place, Saskatoon S7N 5E2, Saskatchewan, Canada*
[c]*Canadian Light Source, University of Saskatchewan, Saskatoon S7N 0X4, Saskatchewan, Canada*
[d]*CERN, Geneva, Switzerland*
[e]*The University of Liverpool, Liverpool, United Kingdom*
[f]*The Australian Synchrotron - ANSTO, Clayton, Australia*

Abstract

A distributed beam loss monitoring system, named the optical fibre Beam Loss Monitor, has been installed at the Australian Synchrotron. Relativistic charged particles produced in beam loss events generate photons via the Cherenkov mechanism in four silica fibres that run parallel to the beam pipe and cover the majority of the accelerator's length. These photons are then guided by the fibres to detectors located outside of the accelerator tunnel. By measuring the time of flight of these photons, the locations of beam losses can be reconstructed. Based on this method a calibration was produced, mapping the time of flight to a position along the accelerator. This calibration was applied to loss signals collected on the first pass of the beam through the accelerator and the locations of prominent losses were determined. Using this system it was possible to investigate the effect, on the location and intensity of losses, in response to changes in the lattice parameters on a shot-by-shot basis. This system is now used in routine operations and has resulted in a 40 % increase in the capture efficiency of the booster ring.

Keywords: Beam Loss Monitor, Distributed BLM, Fibre BLM, Beam Loss Location, Cherenkov BLM

1. Introduction

An understanding of beam behaviour is essential for the operation of particle accelerators. This understanding extends beyond the stored beam to beam that is lost, both deliberately and accidentally, as it traverses the accelerator. Beam Loss Monitors (BLMs) are employed to study these losses and provide valuable information for both machine protection and radiation safety [1].

Optical fibres have been shown to be useful BLMs that can easily cover large lengths of an accelerator [2, 3, 4]. They were originally conceived as a means of economically and efficiently protecting long accelerators from dangerous beam losses. One such system, called the optical fibre Beam Loss Monitor (oBLM), was installed at the Australian Synchrotron as part of the Compact Linear Collider (CLiC) development program [5]. The oBLM was installed to test whether it would be suitable for monitoring beam losses at a future linear collider [6].

This paper presents the process of incorporating the oBLM into the operations of the Australian Synchrotron. It begins with a review and verification of the results of the previous study [6, 7, 8], and then proceeds to discuss the process of re-configuring, calibrating and implementing this system.

1.1. Cherenkov radiation in Fibres

In 1932, Cherenkov first investigated the electromagnetic radiation produced when a charged particle moves faster than the phase velocity of light in a medium [9]. This phenomenon is now referred to as Cherenkov radiation.

*Corresponding author
Email address: pgia@student.unimelb.edu.au (Paul J. Giansiracusa)

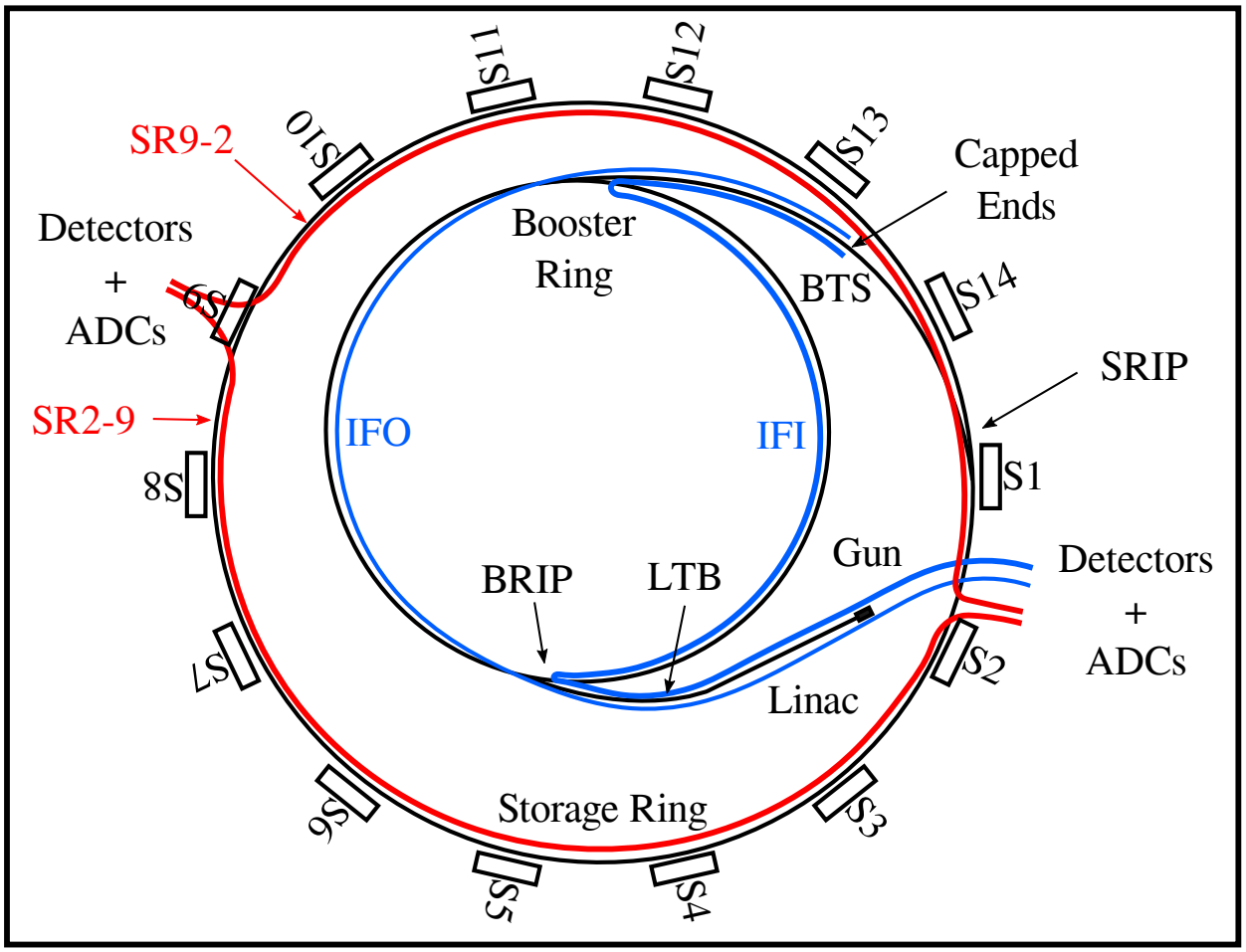

Figure 1: The locations of the four fibres installed at the Australian Synchrotron. The blue lines show the fibres, IFO and IFI, installed along the injection system. The red lines show the fibres, SR2-9 and SR9-2, installed on the storage ring. S1-14 are the fourteen sectors of the storage ring. Only a short section of the booster to storage (BTS) ring transfer line is not covered. BRIP and SRIP correspond to the booster ring and storage ring injection points, respectively.

Leveraging Cherenkov's experimental work, Frank and Tamm [10] were able to produce a theoretical description based on classical electromagnetism.

The underlying mechanism behind the production of Cherenkov radiation proceeds as follows. Consider a charged particle with velocity, v, moving through a dielectric material. As it passes through, atoms within the material are polarised in response to its electric field. If v is less than the phase velocity, v_p, no net dipole field is created. However, if v is greater than the phase velocity, a net dipole field exists and Cherenkov radiation is produced and emitted in a cone with a characteristic angle, θ_c, with respect to the path of the particle given by:

$$\cos\theta_c = \frac{AC}{AB} = \frac{c}{vn}, \tag{1}$$

where AB is the distance travelled by the particle in the time the emitted light travels the distance AC, c is the speed of light, and n is the refractive index of the medium.

Within a material the refractive index is dependent on the dispersion, which results from a variation in the refractive index with respect to the wavelength, λ, of the interacting radiation, such that n becomes $n(\lambda)$. In the case of Cherenkov radiation, this defines the emission spectrum. For many materials, there are regions where $n(\lambda)$ is approximately constant. Such is the case for silica where $n \sim 1.47$ with a variation of less than three percent in the region $\lambda = 900$ to

200 nm [11], which covers the visible spectrum and extends into both the infrared and ultraviolet regions. Thus, the minimum velocity to produce Cherenkov radiation in silica can be calculated by setting $\theta_c = 0$ and $n = 1.47$, giving $v \geq 2.04 \times 10^8$ ms^{-1} or a kinetic energy of $E_k \geq 186$ keV for electrons and positrons.

2. Experimental Setup

The Australian Synchrotron is a 3rd generation light source [12]. The injection system which provides beam to the storage ring consists of a thermionic electron gun, a 100 MeV linac, the linac to booster (LTB) transfer-line, a 3 GeV booster synchrotron and the booster to storage ring (BTS) transfer-line. The storage ring is 216 m in circumference and the beam energy of 3 GeV is maintained with 500 MHz RF producing 2 ns bunch spacing. In user beam operation 300 of the 360 storage ring RF buckets are filled approximately equally with a nominal total current of 200 mA. Top up injections are used to maintain the nominal beam current, with bunch trains approximately 150 ns in length and a total charge of 500 pC injected every 4 minutes. To maintain a flat fill pattern in the storage ring target buckets, spaced 24 ns apart, are stepped through shot-by-shot. Arbitrary fill patterns and single bunch operations are also possible. The storage ring consists of 14 sectors each of which begins with a straight section followed by a double bend achromat lattice cell [12].

The oBLM system consists of four 125 m long silica fibres. They are installed such that they run parallel to the beam pipe and cover the majority of the system, as shown in Figure 1. The fibres are named after the sections of accelerator they cover (Fig. 1) as follows; Storage Ring sectors 2-9 (SR2-9), Storage Ring sectors 9-2 (SR9-2), Injection Fibre Outside (IFO) and Injection Fibre Inside (IFI). Insertion devices and RF Cavities, which the fibres are routed around as best as possible, are installed in Sectors 3, 5, 8, 12, 13 and 14, and in Sectors 6 and 7, respectively. Each fibre is made up of 245 μm silica (SiO_2), 200 μm core and 45 μm cladding, coated in a light tight sheath and then covered by a protective nylon jacket. Light is detected by Multi-Pixel Photon Counters (MPPCs) (Hamamastu s12572-015c), and the signal is digitised using two analogue to digital converters (ADCs) with a front end bandwidth of 600 MHz at 8 bit and 5 GSs^{-1}. Signals can be collected at both ends of SR2-9 and SR 9-2, but only on one end of both IFO and IFI (Fig. 1). The unused ends are capped to ensure no external light can leak in. Signals at the downstream ends of the fibres are likely to pile up, as the beam generating the losses is faster than the signals travelling in the fibres. Therefore, all of the measurements in this work were performed using signals recorded at the upstream end of the fibres. Future work will investigate the use of the downstream ends, for less time critical processes, such as integrated losses.

3. Review

The original motivation for the installation of the oBLM system at the Australian Synchrotron was to test the applicability of the system for use at CLiC [6, 7, 8]. The Australian Synchrotron was an ideal choice as the storage ring can be tuned to operate with parameters similar to those of the damping rings that would form a part of the injection system of the future collider [7]. Several measurements were undertaken by the CLiC collaboration with the aim to measure the temporal resolution and sensitivity of the oBLM, in order to conclude whether it was possible to determine the locations of losses produced by a CLiC-like bunch train. The results of this work can be found in Nebot del Busto et al. [6, 7] and Kastriotou et al. [8]. In this section a review of the key results is presented.

Several photo-sensors including MPPCs, photo-multiplier tubes (PMTs), MSM photo-detectors, avalanche photo-diodes (APDs) and PIN diodes were tested for suitability. It was found that the MPPCs and PMTs provided the greatest dynamic range and lowest noise [6]. The choice was made to use MPPCs over PMTs due to their superior single photon counting capabilities and slightly sharper rise time, 10 ns compared to 15 ns with a beam loss signal [6]. Sensitivity measurements using fibres with a core diameter of 365 μm, larger than those currently installed, showed that losses on the order of a hundred thousand electrons could be seen with the MPPCs and down to tens of thousands with 30 dB amplification [6]. It has been shown that the sensitivity of fibre loss monitors is proportional to the square of the radius [4].

Measurements of losses with single bunch injection were used to probe the time resolution of the oBLM. Loss signals were produced by inserting the beam scrapers, fully blocking the path of the beam. The signals were digitised and the locations of leading edges were compared in post processing to determine timing resolution. It was found that

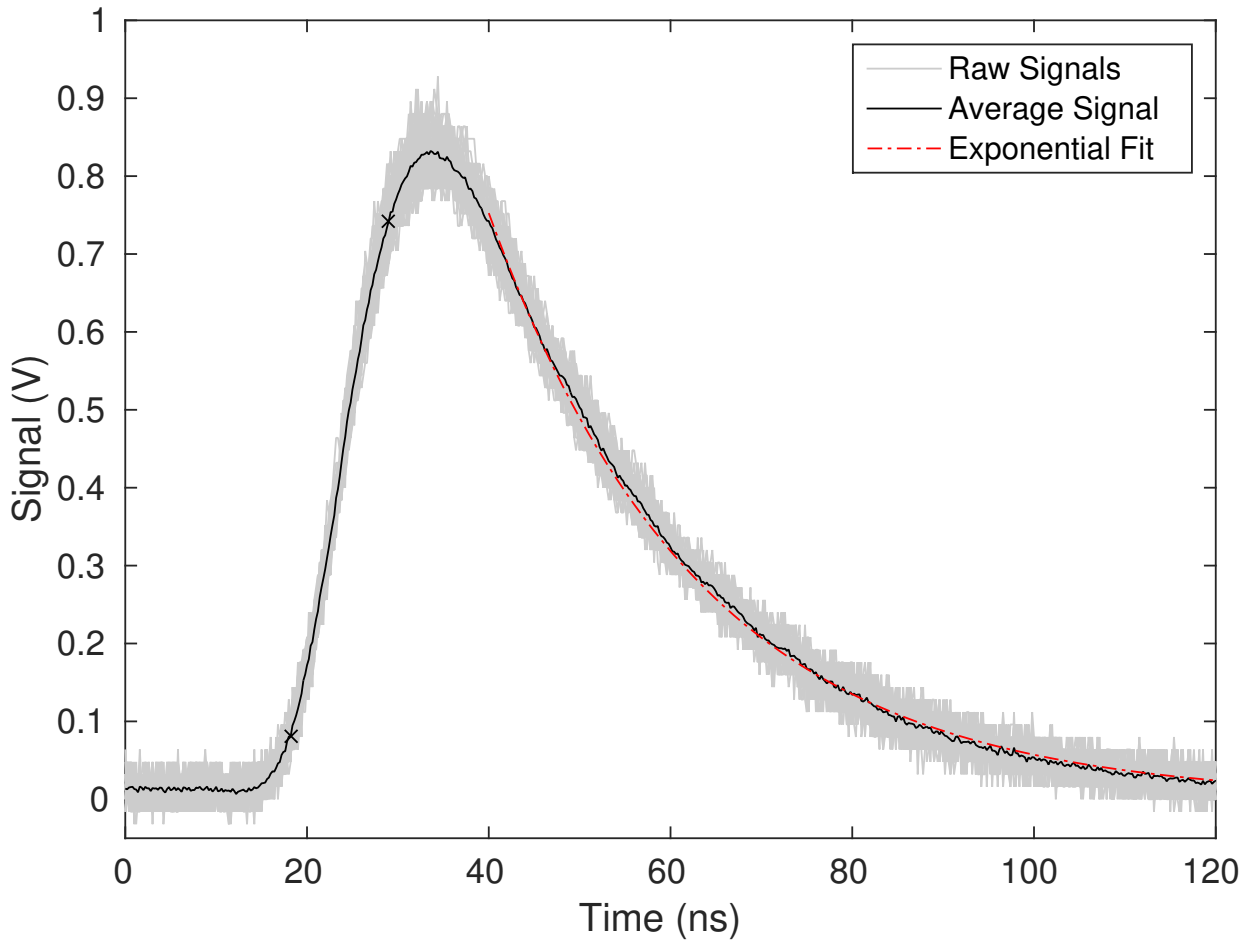

Figure 2: An example of the loss signals recorded by the oBLM for losses generated at the first valve after the SRIP. The grey shading shows 100 signals overlaid on each other and the black trace shows their average. The black crosses show 10% and 90% points and the red trace is an exponential fit of the decaying edge.

losses produced by targeting subsequent RF buckets, 2 ns apart, were easily distinguishable and the overall timing resolution of the oBLM system was determined to be better than 300 ps [7].

Measurements with multi-bunch trains showed loss points with a large spatial separation, on the order of 10 m, could be easily distinguished by the leading edges. However, for loss points with closer separation, on the order of 1 m, as the bunch train length was increased from 30 ns to the nominal CLiC bunch length (at the time) of 150 ns, the signals became increasingly overlapped [7]. Finally, frequency analysis showed that it is also possible to determine the revolution frequency and horizontal and vertical tunes from the loss signals [6].

4. Procedure

The following describes the process of testing and development of the oBLM system specifically for use at the Australian Synchrotron. Several changes were made to the system between the previous study and this work. This includes the replacement of the storage ring fibres, SR2-9 and SR9-2.

4.1. Initial Testing

Initial testing was undertaken to determine the response of the system to losses produced at a known location. This was achieved by inserting a vacuum valve into the path of the beam, effectively using it as a thick scattering target.

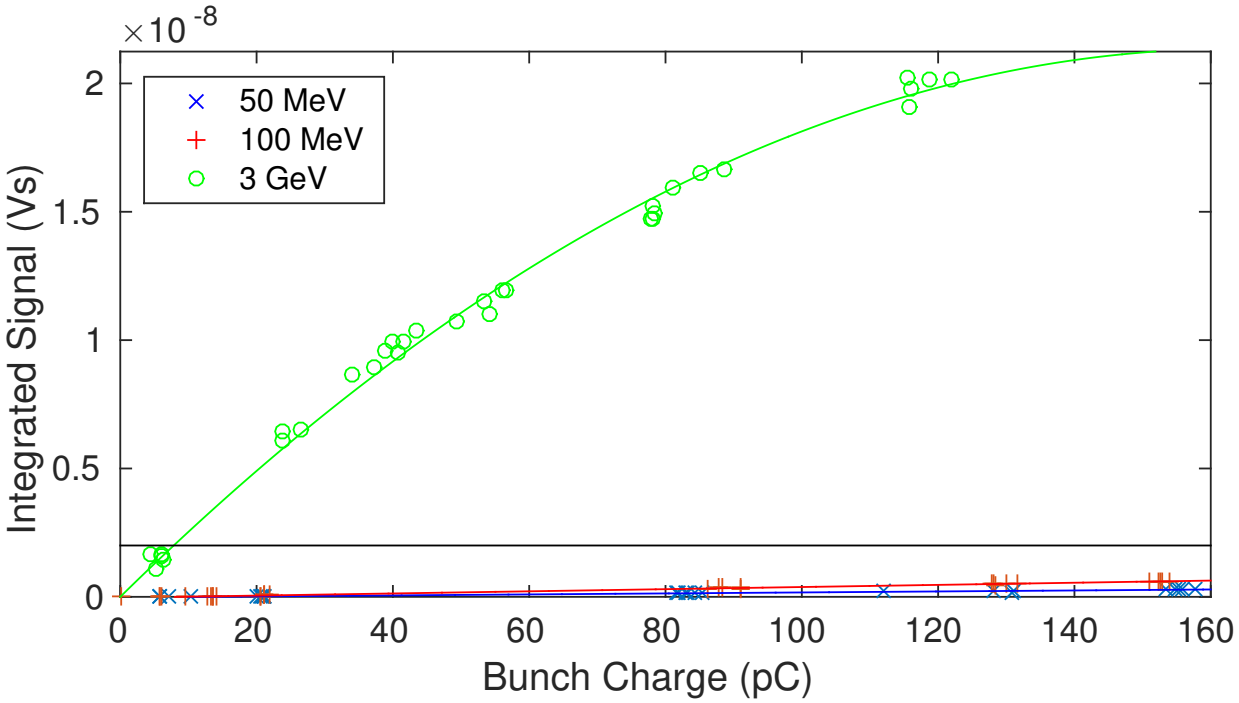

(a) Full scale. The lower rectangle defines the region of interest shown below.

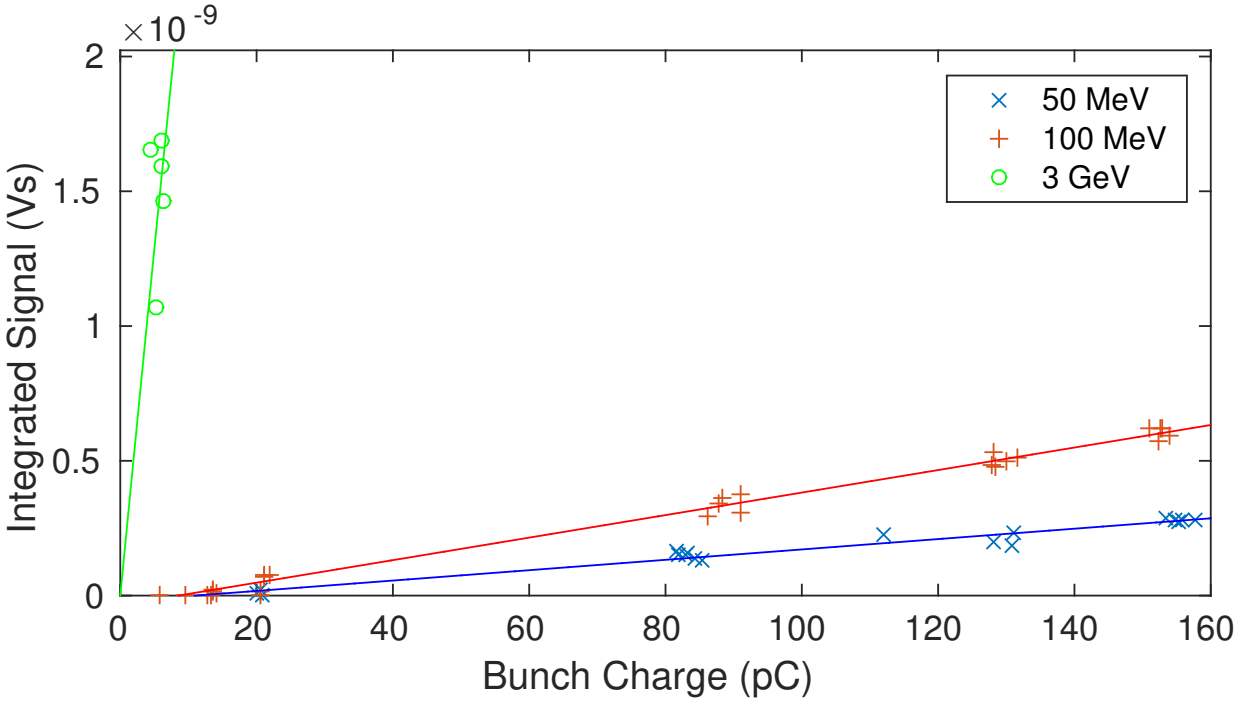

(b) Region of interest.

Figure 3: The sensitivity of the system to beam losses at different energies. The results at 50 MeV, 100 MeV and 3 GeV are shown in blue, red and green, respectively.

This slows the beam via Bremsstrahlung (and other processes) producing an electromagnetic shower at the point of the interaction and in lattice elements down stream of the value where any beam that penetrates is lost, impacting the beam pipe as it no longer has sufficient energy for acceptance.

A single bunch, nominally 3 GeV, 150 pC and with a length of 25 ps, was scattered using the first valve after the SRIP and detected by fibre SR9-2. This process was repeated to produce Figure 2, which shows one hundred raw signals and their average. The signals represent an example of the system response at a single location. They show a repeatable and desired response, with a rise time of 10.8 ± 0.76 ns. An exponential was also fitted to the trailing edge to determine the decay constant of the MPPCs, which was found to be 23.3 ± 0.18 ns. This process was repeated for valves at various locations around the accelerator, and it was found that the rise time varied with the location. Further testing revealed that this variation is uncorrelated with location, and therefore not caused by dispersion which was the initial assumption. It is believed that the signal shape is dependent on the local environment around the loss point; the relative shielding, and distance between it and the fibre.

4.2. System Sensitivity

System sensitivity was measured by injecting single bunches of varying charge into three vacuum valves where beam energies of 50 MeV, 100 MeV and 3 GeV were accessible. A wall current monitor located directly after the thermionic gun and a fast current transformer (FCT) in the BTS, were used to measure the bunch charges. Signals were collected using ADCs and the integrated signal determined in post processing at the full width half maximum. Figure 3 shows the observed response with (a) and (b) showing the full scale and region of interest, respectively. It can be seen that the signal strength increases with both bunch charge and energy. The signals at 3 GeV begin to saturate the MPPC at approximately 40 pC, and thereafter a non linear response is observed. The smallest bunch charges detectable by the FCT at 3 GeV produced signals greater than the largest bunch charges at 100 MeV, Fig. 3 (b). Despite reaching the limit of the FCT, signals were still observable from the fibre, demonstrating their sensitivity. A second order polynomial was fitted to the 3 GeV data, shown in solid green (Fig. 3). The fitted function was used to determine the bunch charge of the smallest signals seen on the fibre, and thus the smallest detectable loss, which was found to be less than 200 fC or on the order of a million electrons, slightly lower than the previous results with larger fibres.

In the preceding section it was discussed that the signal shape is observed to vary with location, this suggests that the sensitivity also varies. An estimate on the variation of the sensitivity was made using data collected in the following sections. Single bunch injections of 90 pC targeting each of the valves along the length of fibre SR2-9 were collected the mean intensity was found to be 1.33×10^{-8} Vs with a standard deviation of 2.7×10^{-9} Vs. This amounts to a location dependant variation of twenty percent.

4.3. Loss Location

It is possible to determine the location of losses along the length of the accelerator by measuring the time of flight (ToF) of the loss signals produced in the fibre. Throughout this work ToF is defined as the time between the triggering of the thermionic gun and the measurement of a leading edge at the upstream end of the corresponding fibre, minus the appropriate delays which account for the time taken for the beam to enter the respective section of the accelerator under investigation. The leading edge position is used for the ToF measurement as it is independent of the bunch train length. A method to reliably determine the position of leading edges was developed, which makes use of a threshold scan and fitting procedure to find leading edges and determine the point of steepest ascent. The leading edge approach relies on the assumption that the leading bunch in a bunch train always contributes to the loss signal. Thus, the signal leading edge uniquely corresponds to the leading bunch. This assumption is based on the results of previous work that showed the position of the leading edge was unchanged as the bunch train length was increased [7].

To understand how the ToF changes with position along the fibre, consider two losses at locations x_1 and x_2 with measured ToF t_1 and t_2, respectively, as shown in Figure 4. The difference in the measured ToF, $\Delta t = t_2 - t_1$, is given by the time it takes the beam to travel from x_1 to x_2, plus the time it takes the signal to travel back to x_1, such that:

$$\Delta t = \frac{\Delta x}{c} + \frac{\Delta x}{v_s} = \frac{\Delta x}{v_{eff}}, \tag{2}$$

where $\Delta x = x_2 - x_1$, v_s is the speed of the signal in the fibre and v_{eff} is the effective velocity observed, which is a useful quantity for determining the expected ToF. In the case of silica fibres $v_{eff} = 0.1214$ m ns^{-1}.

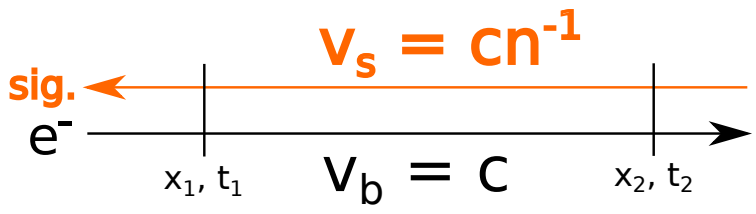

Figure 4: A simplified diagram showing, the propagation of the beam, black, and the signal, orange, for losses at two locations x_1 and x_2.

The accuracy of the loss locations determined by means of the ToF can be improved with a calibration that maps the ToF to loss signals generated at known locations. Such a calibration was produced, for each of the fibres, by targeting each vacuum valve along the length of the accelerator in turn. Single bunch injections of 90 pC were scattered by the valves with beam energies of 100 MeV and 3 GeV for the injection system and storage ring fibres, respectively. The evolution of the signals observed by SR2-9, as this procedure was preformed, can be found in Figure 5. It can be seen that the signal's position in time increases as valves further along the accelerator are inserted. It is also evident, as discussed earlier in Section 4.1, that the rise time and the structure of the signals is different at each location. Furthermore, the double-peak structure seen in Figure 5 appears to be systematic from valve to valve, with the double-peak structures appearing to overlap for valves in the same sector. Measurement of the leading edges yields a spacing of approximately 3.2 m. This is consistent with the spacing between the first two quadruples in each lattice cell of 3.26 m, suggesting that a significant portion of the beam penetrates the valve and is lost in the subsequent regions of high field. Similar results exist for the three remaining fibres and have been used to create the calibrations that follow.

The resulting calibrations for the two injection system fibres, IFO and IFI, are shown in Figure 6. The two fibres show good agreement along the linac and LTB where they run parallel to each other (the results for IFI have been offset by 10 ns for clarity). IFO then continues along the first half of the booster ring and the expected linear relationship is seen. Since the current setup only allows for light to be collected at one end of the fibres on the injection system, the only upstream signals for IFI come from the first three valves in the system along the linac and LTB (Fig. 1), and any losses produced in the second half of the booster ring will result in downstream signals at the accessible end.

Presented in Figure 7 are the calibrations for the two storage ring fibres, SR2-9 and SR9-2. As with the injection system fibres, the expected linear relationship is seen. A linear fit of the data is shown, the gradient of which is 8.17 ± 0.11 ns m^{-1} consistent with $v_{eff}^{-1} = 8.24$ ns m^{-1}. When installing the fibres an effort was made to ensure they followed the beam pipe as best as possible, however there are regions where they had to be routed around various obstacles, such as insertion devices and RF cavities, resulting in the deviations from linearity seen in Figure 7. It is possible to account for these deviations as each valve location is known to millimetre accuracy. Therefore, instead of calibrating each of the fibres using a global linear fit, a linear interpolation between the observed ToF for any two adjacent vales is used.

In the case of SR9-2 there is a short section at the end of the fibre, from the storage ring injection point (SRIP) to Sector Two (Fig. 1), that is exposed to the beam before what is considered the beginning of the fibre in Sector Nine. Since any signals produced in this region take longer to reach the beginning of the fibre than the beam travelling in the opposite direction around the storage ring, there exists a degeneracy in the measured ToF. Specifically, any signals produced between the SRIP and Sector Two will have a ToF indistinguishable from signals produced in Sector Nine and part of Ten. This can be observed, in Figure 7, in the measured ToF for the valves in Sector One, at 0 and 10.58 m. Also, under conditions where the beam is allowed to make more than one turn of the storage or booster rings, similar ToF degeneracies are possible in the other fibres. Since, losses originating near the start of a fibre on the second turn have a ToF equal to losses originating near the end of the fibre on the first turn. Such degeneracies create ambiguities that must be taken into account when assigning a location to a detected loss.

After calibrating each of the fibres, the locations of losses produced by the beam on its first pass through the accelerator could be determined. Several hundred loss signals were collected for all four fibres during single bunch and multi-bunch operations. The average signals for each combination of fibre and operating mode are plotted in Figure 8, with points of interest and degenerate regions marked. The calibrations produced earlier were used to scale the horizontal axes of the plots allowing the locations of losses to be determined from the plots by the leading edges.

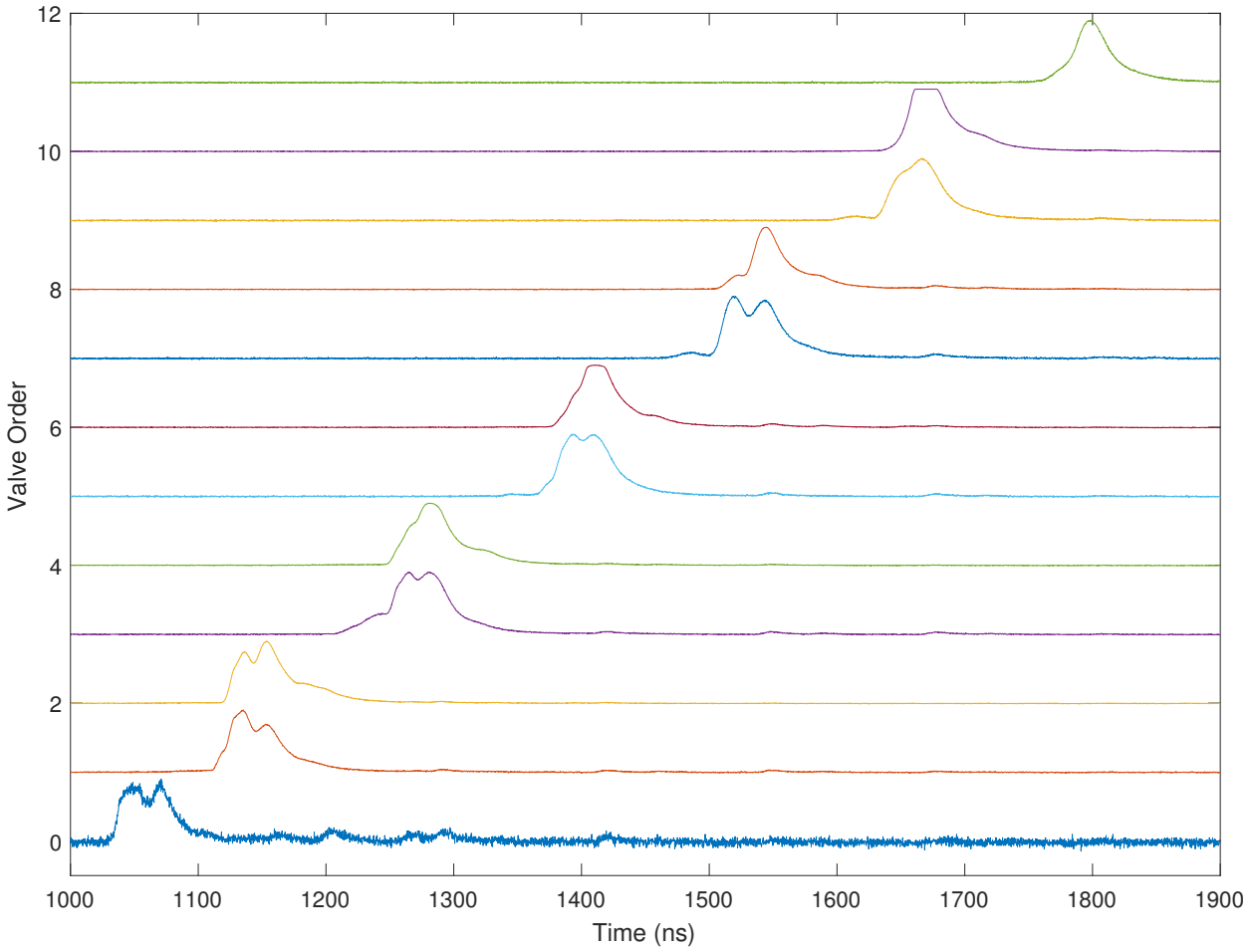

Figure 5: A waterfall plot showing the raw signals produced by each valve for SR2-9 and used to create the calibration. Each of the signals has been normalised to its maximum.

In the multi-bunch case the signals were collected during user beam operation, with the beam parameters as described in Section 2. Whereas, in the single bunch case the last valve in Sector Fourteen was closed to ensure the beam did not begin a second turn and the nominal beam parameters described in Section 4.1 were used.

The data presented in Figure 8 (a) reveals that significant losses occur along the injection system after the end of the linac and along the entire length of the LTB. These losses gradually diminish as the beam enters the booster ring. In the case of the multi-bunch signals, as expected, IFO sees a stronger signal than IFI as it runs on the outside of the beam pipe. However, this is not evident in the single bunch signals, with a prominent peak present just after the linac in the IFO signal (note the single bunch signals have been scaled by a factor of five). It was hypothesised that this peak was caused by a large energy spread in the single bunch beam at the end of the linac, with a prominent low energy tail, prompting a measurement of the linac's energy spread. While attempting this measurement it was found that the lower blade of the energy defining slits (which are no longer used in operation) was partially inserted, explaining the observed peak.

A significant difference is observed between the single bunch and multi-bunch signals detected by SR2-9 on the first pass of the beam through the accelerator (Fig. 8 (b)). No losses are observed in the single bunch signals and only small (note the difference in vertical scale between Figure 8 (b) and (c)) losses are observed in the multi-bunch signals. The multi-bunch losses are observed in Sectors Two, Three and Five. Losses in these sectors are attributed to the devices installed in these sectors that are not present in the later sectors that see no losses. As such, the signals are attributed to losses at the injection kicker in Sector Two and at the aperture changes of the in-vacuum undulators

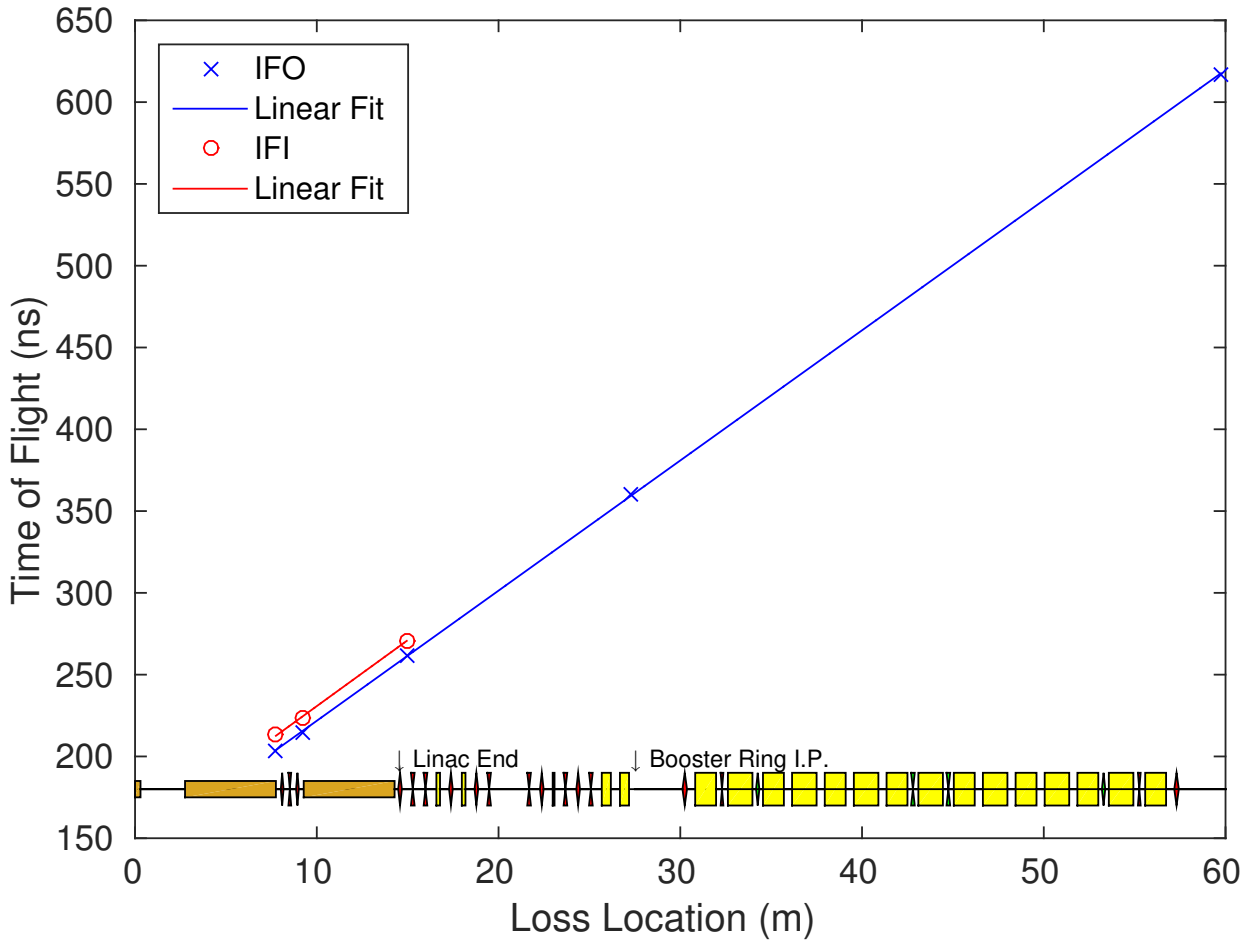

Figure 6: The resulting calibrations for the injection system fibres, IFI and IFO. Locations are given relative to the thermionic gun. A sketch of the lattice elements that the beam passes is shown on the horizontal axis. Blue and red are the results for the outside fibre (IFO) and inside fibre (IFI), respectively. The results for IFI have been offset vertically by 10 *ns* for clarity.

(IVUs) in Sectors Three and Five.

Finally, the signals observed by SR9-2 as the beam completes its first pass through the accelerator are shown in Figure 8 (c). The first peak found in both single bunch and multi-bunch signals falls in the degenerate region, therefore it could either be produced by losses in sector nine, as shown, or by losses between the SRIP and the end of the fibre as described earlier. In order to decide between these two cases a signal collected with the first valve in Sector One closed was also plotted. It can be seen that a similar peak exists just before the much larger peak produced by the closed valve. Thus, the first peaks for both the single and multi-bunch signals are attributed to injection losses in Sector One. The second peak, similarly occurring in all cases, is understood to be the downstream light from the event that produced the previous peak reflected from the end of the fibre. Finally, the last peaks observed in the single bunch and multi-bunch signals are attributed to the closed valve in Sector Fourteen and a loss in the region of the SRIP produced by the beam on the second turn, respectively.

In consideration of the results presented and the potential to measure degenerate ToF, it is evident that the current fibre layout is not optimal for determining loss locations. Ideally, the setup would be such that the time required by the beam to travel the length of accelerator not covered by the fibre be greater than the time for a signal to travel the length of the fibre. For a circular section of accelerator this requires that:

$$\text{Length of the Fibre} < \frac{\text{Circumference of the Ring}}{\text{Refractive Index} + 1} \tag{3}$$

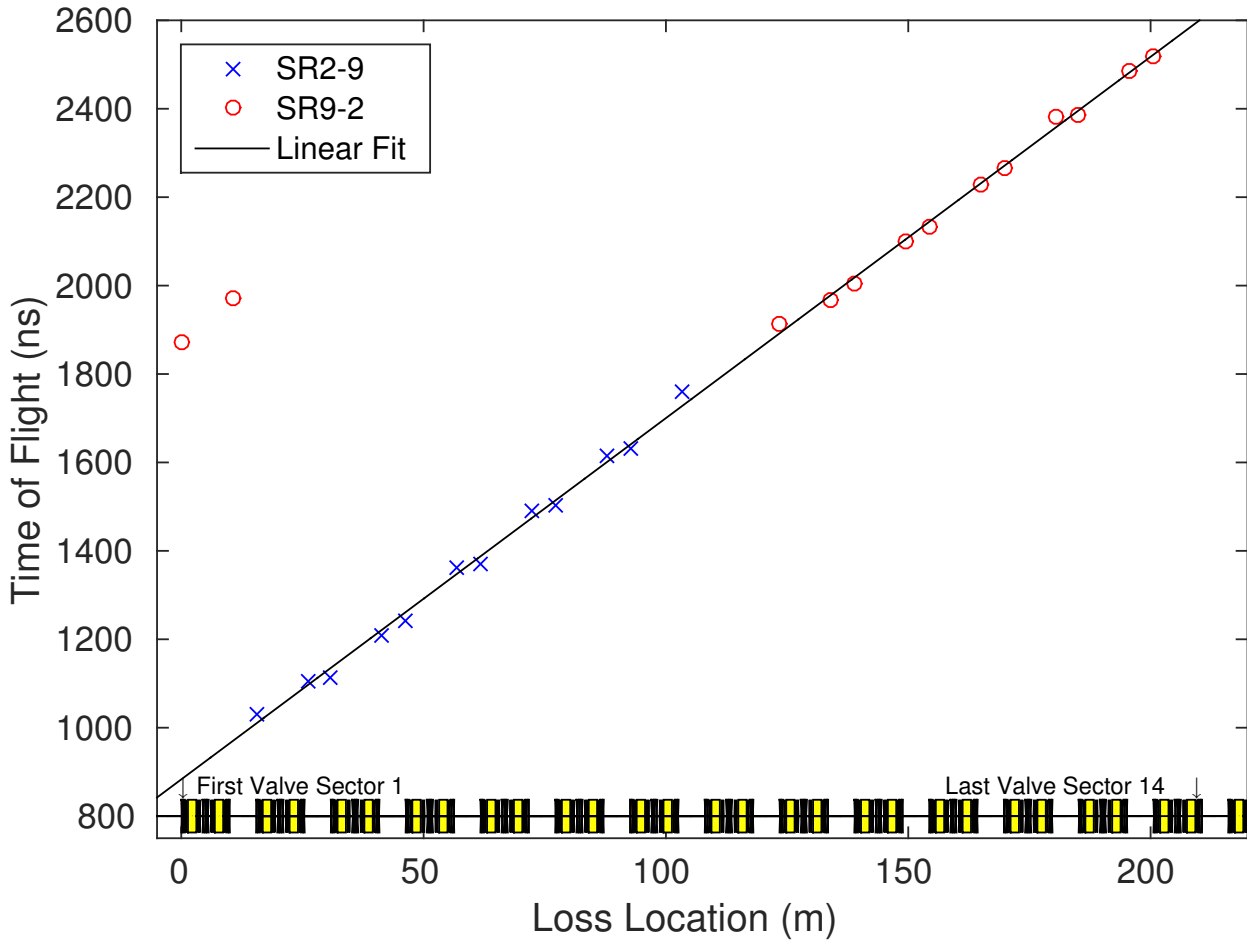

Figure 7: The resulting to calibrations for the storage ring fibres, SR2-9 and SR9-2. A sketch of the lattice elements that the beam passes is shown on the horizontal axis. Locations are given relative to the first valve in Sector One. Blue crosses show the results for the fibre covering sectors two to nine and red points sectors nine to two.

Thus, a minimum of three equal length silica fibres is required to cover a circular section of accelerator. Furthermore, the case of reflected signals can be avoided by setting the appropriate time window on the ADC for the first pass of the beam by ensuring the beginning of the first fibre is at the injection point of the ring. This being the case, the only assumption when determining a loss location is that the signal's leading edge uniquely corresponds to the leading bunch.

4.4. Injection Efficiency

The injection efficiency monitoring system of the Australian Synchrotron has now been extended to include the automated analysis of data from the oBLM. A new feature is a diagnostic display which reports the position and intensity of losses which occur in the linac, LTB and booster ring. This provided operators with an opportunity to observe effects of lattice parameter adjustments on the losses in real-time. Using these new diagnostics, the lattice was optimised and the capture efficiency into the booster ring was improved by 40 % over the previous operating parameters. It is anticipated that with the addition of a fibre to the BTS, it will be possible to optimise capture into the storage ring as well, further improving the injection efficiency.

5. Conclusion

The optical fibre Beam Loss Monitor was successfully calibrated and integrated into the operations of the Australian Synchrotron. Measurements showed loss signals at a test location had a rise time of 10.8 ± 0.76 ns and the system was sensitive to losses on the order of a million electrons. A calibration was produced, mapping the loss location to the signal time of flight, and allowing the location of losses produced by the beam on its first pass through the accelerator to be determined. Significant losses were found to occur at various locations during injection, particularly around injection points. The limitations of using the oBLM for the determination of loss location were discussed, in particular the case of long fibres leading to degeneracies in the measured ToF. To overcome these limitations, it is recommended that a minimum of three equal length silica fibres be used to cover a circular section of accelerator. Finally, the oBLM system is now used in routine operations and has resulted in a 40 % increase in the capture efficiency of the booster ring.

Acknowledgements

The authors would like to thank the Operators and Physics staff of the Australian Synchrotron for their helpful discussions and willingness to generate beam losses.

References

[1] K. Wittenburg, Beam loss monitors, CERN Accelerator School: Course on Beam Diagnostics (2009) 249.
[2] E. Janata, M. Körfer, Radiation detection by Cerenkov emission in optical fibers at TTF, Technical Report, Dt. Elektronen-Synchrotron DESY, MHF-SL Group, 2000.
[3] A. Pietryla, W. Berg, R. Merl, A cerenkov radiation detection system for the advanced photon source storage ring, in: Particle Accelerator Conference, 2001. PAC 2001. Proceedings of the 2001, volume 2, IEEE, pp. 1622–1624.
[4] J. W. van Hoorne, Cherenkov Fibers for Beam Loss Monitoring at the CLIC Two Beam Module, Technical Report, 2012.
[5] M. Aicheler, P. Burrows, M. Draper, T. Garvey, P. Lebrun, K. Peach, N. Phinney, H. Schmickler, D. Schulte, N. Toge, A Multi-TeV linear collider based on CLIC technology: CLIC Conceptual Design Report, Technical Report, SLAC National Accelerator Lab., Menlo Park, CA (United States), 2014.
[6] E. Nebot del Busto, *et al.*, Measurement of beam losses using optical fibers at the australian synchrotron, in Proc. 3rd International Beam Instrumentation Conference, Monterey, CA, USA (2014) 515520.
[7] E. Nebot del Busto, M. J. Boland, S. Doebert, F. Domingues, E. Effinger, W. Farabolini, E. B. Holzer, M. Kastriotou, R. Rassool, W. Vigano, et al., Position resolution of optical fibre-based beam loss monitors using long electron pulses, Proc. IBIC15 (2015) 580–584.
[8] M. Kastriotou, M. Boland, E. B. Holzer, E. Nebot del Busto, C. Welsch, An optical fibre blm system at the australian synchrotron light source, in: 5th Int. Beam Instrumentation Conf.(IBIC'16), Barcelona, Spain, Sept. 13-18, 2016, JACOW, Geneva, Switzerland, pp. 670–673.
[9] P. Čerenkov, Visible radiation produced by electrons moving in a medium with velocities exceeding that of light, Physical Review 52 (1937) 378.
[10] I. Tamm, I. Frank, Coherent radiation of fast electrons in a medium, in: Dokl. Akad. Nauk SSSR, volume 14, pp. 107–112.
[11] I. Malitson, Interspecimen comparison of the refractive index of fused silica, Josa 55 (1965) 1205–1209.
[12] J. Boldeman, D. Einfeld, The physics design of the australian synchrotron storage ring, Nuclear Instruments and Methods in Physics Research Section A: Accelerators, Spectrometers, Detectors and Associated Equipment 521 (2004) 306–317.

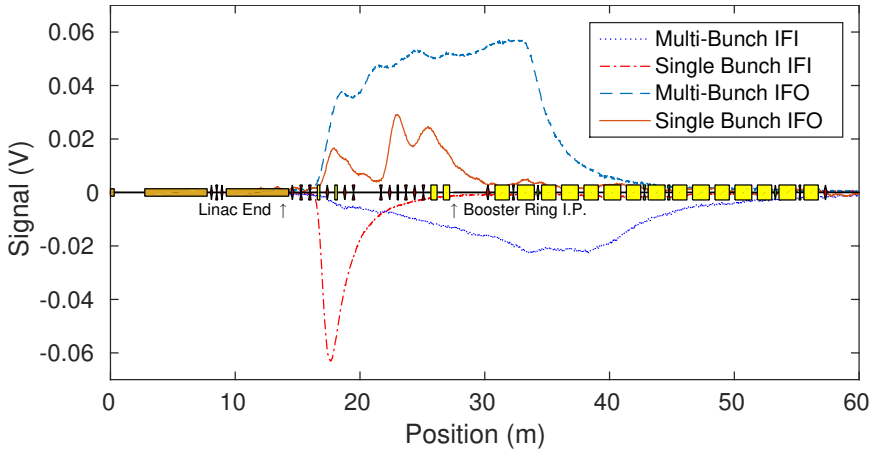

(a) The loss signals observed by the injection system fibres, IFI and IFO, on the first pass of the beam. The red and orange traces show the single bunch results, scaled by a factor of five, for IFI and IFO, respectively and the blue and light blue traces show the multi-bunch signals for IFI and IFO, respectively. The signals observed by IFI have been inverted for clarity.

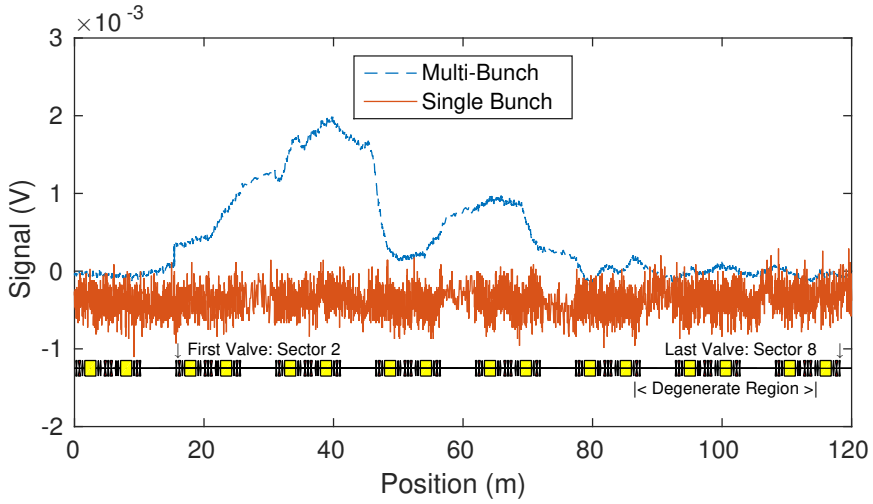

(b) The loss signals observed by SR2-9 on the first pass of the beam. The red and blue traces show the single bunch and multi-bunch signals, respectively. In the single bunch case no discernible signals are observed. The first and last valves the fibre passes have been marked and the degenerate region is highlighted.

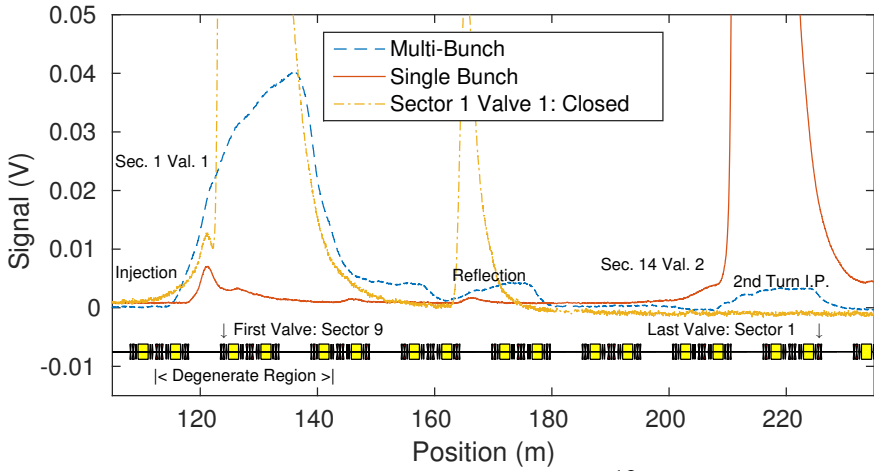

(c) The loss signals observed by SR9-2 on the first pass of the beam. The red and blue traces show the single bunch and multi-bunch signals, respectively. The yellow trace shows the signal with the first valve in the storage ring closed. In the single bunch case the last valve in the system, valve two in Sector Fourteen, was closed to ensure the beam did not begin a second turn. The first and last valves the fibre passes have been marked and the degenerate region is highlighted.

Figure 8: The loss signals observed on the first pass of the beam for single bunch and multi-bunch injections. Models of the lattice elements, at their respective positions, are shown along the horizontal axes.